

# CrystEngComm

Accepted Manuscript



This is an *Accepted Manuscript*, which has been through the Royal Society of Chemistry peer review process and has been accepted for publication.

*Accepted Manuscripts* are published online shortly after acceptance, before technical editing, formatting and proof reading. Using this free service, authors can make their results available to the community, in citable form, before we publish the edited article. We will replace this *Accepted Manuscript* with the edited and formatted *Advance Article* as soon as it is available.

You can find more information about *Accepted Manuscripts* in the [Information for Authors](#).

Please note that technical editing may introduce minor changes to the text and/or graphics, which may alter content. The journal's standard [Terms & Conditions](#) and the [Ethical guidelines](#) still apply. In no event shall the Royal Society of Chemistry be held responsible for any errors or omissions in this *Accepted Manuscript* or any consequences arising from the use of any information it contains.

## ARTICLE

## Introduction of peroxy groups into titania: Preparing, characterization and properties of the new peroxy-containing phase

Cite this: DOI: 10.1039/x0xx00000x

Received 00th January 2012,  
Accepted 00th January 2012

DOI: 10.1039/x0xx00000x

www.rsc.org/

E. V. Savinkina,<sup>a</sup> L. N. Obolenskaya,<sup>a</sup> G. M. Kuzmicheva,<sup>a</sup> E. N. Kabachkov,<sup>b,c</sup>  
A. A. Gainanova,<sup>a</sup> Y. V. Zubavichus,<sup>d</sup> V. Y. Murzin<sup>d</sup> and N. V. Sadovskaya<sup>e</sup>

The new phase, where peroxy groups are incorporated into titania particles, along with anatase and hydrated  $\eta$ -TiO<sub>2</sub> with peroxy groups on the surface of titania nanoparticles, were prepared by introduction of H<sub>2</sub>O<sub>2</sub> into reaction mixtures while synthesizing TiO<sub>2</sub> from TiOSO<sub>4</sub> or by cold impregnation of pre-synthesized TiO<sub>2</sub>. The samples were studied by a complex of methods (classical and synchrotron-radiation X-ray powder diffraction, small-angle X-ray scattering, high-resolution scanning electron microscopy with energy-dispersive X-ray spectroscopy, X-ray absorption spectroscopy, IR and Raman spectroscopy, X-ray photoelectron spectroscopy, UV-vis diffuse reflectance and absorption spectroscopy, DSC). The [TiO<sub>x</sub>(O<sub>2</sub>)<sub>2-x</sub>(H<sub>2</sub>O)<sub>m</sub>] phase was first structurally characterized and compared to  $\eta$ -TiO<sub>2</sub>. Most samples of H<sub>2</sub>O<sub>2</sub>-sensitized TiO<sub>2</sub> discolor methyl orange under visible light irradiation faster than commercial Hombikat UV100 treated with H<sub>2</sub>O<sub>2</sub>. The activity of the samples strongly relating to their phase composition was associated with existence of large amount of titanium peroxy complexes along with formation of mixed-phase samples.

### Introduction

Titanium dioxide is a wide band-gap semiconductor that can be excited to produce electron-hole pairs when irradiated with light. Such photo-induced electron-hole pairs have been used to generate electricity in solar cells, to split water into hydrogen and oxygen, to oxidize and degrade inorganic/organic/biological compounds in environments as well as to create superhydrophilicity.<sup>1</sup> Among many candidates for photocatalysis, TiO<sub>2</sub> is almost the only material suitable for industrial use.<sup>2-5</sup> The most well-known TiO<sub>2</sub> crystal structures, rutile, brookite and anatase, are commonly used as photocatalysts, with anatase showing greater photocatalytic activity for most reactions.<sup>6-8</sup> The differences in lattice structures of anatase and rutile cause different densities and electronic band structures, leading to different band gaps (3.20 and 3.02 eV for bulk anatase and rutile, respectively).<sup>9</sup> Recently obtained nanosize " $\eta$ -TiO<sub>2</sub>", which small crystals when contacted with electrolyte solutions and vapors, water for example, generate plethora of surface hydroxyl groups, highly reactive towards adsorption reactions with contaminant

molecules and ions, is a promising material for sorption and (photo)catalysis.<sup>10</sup>

Visible-light activated TiO<sub>2</sub> can be prepared by doping or sensitizing with dyes.<sup>11,12</sup> However, dye sensitization is usually accompanied by such problems as dye desorption and decomposition.<sup>13</sup> Titanium(IV) is known to form colored peroxy compounds, their color and stability depending on pH.<sup>14,15</sup> Therefore, peroxide can be used for sensitizing titania. Hydrogen peroxide was often applied to disperse titania particles. Thus, it was used as a coordination agent to leach Ti from the hydrolyzed titania residue prepared from natural titanium minerals; the peroxy-titania powder prepared by boiling the aqueous titanium peroxide solution was crystalline anatase phase; a well-crystallized anatase and rutile could be obtained through calcining at the temperature of 800 and 1000°C, respectively.<sup>16</sup> Hydrogen peroxide is widely used in catalysis and photocatalysis fields to obtain nanosized TiO<sub>2</sub> thin film.<sup>17-19</sup> Anatase nanocrystals were obtained by hydrothermal treatment of water-soluble titanium complexes prepared by addition of a complexing agent such as glycolic acid or citric acid to the yellow transparent solution containing the titanium-peroxy complex.<sup>20</sup> Formation of spindle-type, monodispersed

anatase nanorods from a peroxotitanate solution without the use of organics is reported; the initial amorphous gel was converted to anatase titania rods using ammonia as a shape controller.<sup>21</sup> For preparing titania powders or films, some authors used peroxo titanic acid pre-synthesized from titanium tetrachloride, titanyl sulfate or tetrabutoxytitanium(IV).<sup>22-26</sup> Annealing of the products destroyed peroxo complexes, therefore the resulting samples showed no photocatalytic activity under visible light. However, annealing of thin films prepared from peroxotitanic acid produced anatase, which was active under visible light in the reaction of decolouration of methyl orange (MO).<sup>27</sup> Recently, we have found decolouration of methyl orange for the samples prepared by cold impregnation and by introduction of H<sub>2</sub>O<sub>2</sub> solutions into reaction mixtures while preparing TiO<sub>2</sub> from solvated TiOSO<sub>4</sub>.<sup>28</sup> The purpose of the work was to prepare titania containing peroxo groups both on the surface and in the bulk of titania nanoparticles and to find correlations between conditions of preparing samples of nano-titania modified with H<sub>2</sub>O<sub>2</sub>, their characteristics and properties.

## Experimental

### Chemicals

Titanyl sulfate (TiO)SO<sub>4</sub>·2H<sub>2</sub>O (technical grade) and (TiO)SO<sub>4</sub>·xH<sub>2</sub>SO<sub>4</sub>·yH<sub>2</sub>O (for synthesis) was purchased from Sigma Aldrich. Other reagents were analytical grade. All commercial reagents were used without further purification. Concentration of H<sub>2</sub>O<sub>2</sub> solutions was monitored by titration with KMnO<sub>4</sub>.

### Synthetic procedures

Sample **1** was prepared by suspending self-made anatase (0.25 g) in 50 mL H<sub>2</sub>O<sub>2</sub> (10 M). The reaction mixture was stirred at room temperature for 40 min. The resulting powder was filtered off, washed with water and acetone and dried at room temperature. Nanosized anatase for sample **1** was prepared by the earlier reported procedure.<sup>29</sup>

Sample **2** was prepared by heating the mixture of 5.00 g TiOSO<sub>4</sub>·2H<sub>2</sub>O and 50 mL H<sub>2</sub>O up to 90°C followed by stirring at 90–95°C for 40 min and at 79–81°C for 220 min, addition of 10 mL H<sub>2</sub>O<sub>2</sub> (10 M) and stirring at 79–81°C for 40 min. In several days, the solid was filtered off, washed with water and acetone and dried at 90°C for 1 h. Sample **3** was prepared similarly, but 3 mL NaOH (0.1 M) were added along with H<sub>2</sub>O<sub>2</sub>.

Sample **4** was prepared by heating the mixture of 4.32 g TiOSO<sub>4</sub>·2H<sub>2</sub>O, 40 mL H<sub>2</sub>O and 2 mL conc. H<sub>2</sub>SO<sub>4</sub> up to 90°C and stirring at 88–93°C for 28 min followed by addition of 25 mL Cs<sub>2</sub>SO<sub>4</sub> (0.4 M) and 3 mL H<sub>2</sub>O<sub>2</sub> (1 M). In several days, the resulting powder was filtered off, washed with water and acetone and dried at 90°C for 1 h. Sample **5** was prepared by re-dispersion of sample **4** in 25 mL NaOH (0.1 M).

Sample **6** was prepared by heating the mixture of 7.35 g TiOSO<sub>4</sub>·xH<sub>2</sub>SO<sub>4</sub>·yH<sub>2</sub>O and 40 mL H<sub>2</sub>O up to 87°C and stirring at 86–90°C for 15 min followed by addition of 54 mL conc.

HCl and 2 mL H<sub>2</sub>O<sub>2</sub> (9 M). In several days, the resulting powder was filtered off, washed with water and acetone and dried at 90°C for 1 h. Sample **7** was prepared similarly, but 30 mL KCl (4.5 M) and 10 mL EDTA (5·10<sup>-4</sup> M) were added along with H<sub>2</sub>O<sub>2</sub>.

Sample **8** was prepared by grinding the mixture of TiOSO<sub>4</sub>·2H<sub>2</sub>O (5 g) and 10 mL of H<sub>2</sub>O<sub>2</sub> (8.5 M), which was pre-cooled down to -21°C, followed by treatment with 50 mL H<sub>2</sub>O, heating up to 90°C and stirring at 90–95°C for 40 min and 79–81°C for 260 min. In several days, the solid was filtered off, washed with water and acetone and dried at room temperature. Samples **9** and **10** were prepared similarly, but with the use of 10 M and 21 M H<sub>2</sub>O<sub>2</sub>, respectively.

Sample **11** was prepared by stirring the mixture of TiOSO<sub>4</sub>·2H<sub>2</sub>O (2.16 g) and 100 mL of H<sub>2</sub>O<sub>2</sub> (10 M) for 90–105 min with self-heating up to 100°C. In several days, the solid was filtered off, washed with water and acetone and dried at room temperature.

### Characterization

X-ray diffraction (XRD) patterns were recorded with sample rotation on an HZG-4 (planar graphite monochromator) diffractometer: CuK<sub>α</sub> radiation in the diffracted beam, stepwise mode (counting time 10 s, a step of 0.02°, 2θ = 2–50°). The intensity data set was reduced using the PROFILE FITTING V 4.0 software package.<sup>30</sup> The crystallite sizes were calculated using the Warren formula:<sup>31</sup>  $D = K\lambda/\beta\cos\theta$ ; where  $\lambda = 1.54051 \text{ \AA}$ ,  $2\theta \sim 25^\circ$  ( $d \sim 3.5 \text{ \AA}$ ; anatase, reflection 101) and  $\sim 27.5^\circ$  ( $d \sim 3.25 \text{ \AA}$ ; rutile, reflection 110),  $\beta$  is the widening of the reflection about instrumental width ( $\beta = [(F_{\text{WHM}})_{\text{exp}}]^2 - (F_{\text{WHM}})_{\text{R}}]^2$ ), where  $(F_{\text{WHM}})_{\text{exp}}$  and  $(F_{\text{WHM}})_{\text{R}}$  are the measured diffraction peak widths at half height for TiO<sub>2</sub> and the  $\alpha$ -Al<sub>2</sub>O<sub>3</sub> standard, respectively),  $K$  (the Scherrer coefficient characterizing crystallite shape) was set to 0.9. Standard deviation was  $\pm 5\%$ . The anatase content in the rutile-containing samples was calculated using the equation:  $x_{\text{R}} (\%) = [1 + 0.65(I_{\text{A}}/I_{\text{R}})]^{-1}$ ,  $x_{\text{A}} (\%) = 100 - x_{\text{R}}$ , where  $I_{\text{A}}$  and  $I_{\text{R}}$  are integral intensities of anatase reflection 101 and rutile reflection 110.

We also used synchrotron radiated X-ray powder diffraction (SR-XRPD) and X-ray absorption spectroscopy at the K edge of titanium. The measurements were carried out at the “Structural Materials Science” end-station installed at the Kurchatov synchrotron radiation source.<sup>32,33</sup> The X-ray diffraction patterns were measured in a transmission geometry (Debye-Scherrer) using Fujifilm phosphor imaging plates coated with a storage layer as an area detector. The X-ray beam size was 200×200 μm<sup>2</sup>, the wavelength  $\lambda = 0.68886 \text{ \AA}$ , the sample-to-detector distance was 150 mm, and the exposure time was 15 min. The imaging plates were digitized using a Fuji BAS-5000 scanner with a step of 100 μm. Two-dimensional diffraction patterns were integrated into standard  $I(2\theta)$  patterns with the Fit2D software package.<sup>34</sup> The integration was carried out applying corrections for the deviation of the phosphor imaging plate from the perpendicular orientation with respect to the X-ray beam, the precise shape of

the integration region, and the linear polarization of synchrotron radiation. The angular scale of the diffraction patterns was calibrated using the polycrystalline NIST SRM640c standard Si.

Small angle X-ray scattering data were recorded on a special SAXSess instrument (Anton Paar, Austria;  $\text{CuK}\alpha$  radiation,  $\lambda = 1.5418 \text{ \AA}$ , linear collimation, collection time 3 min, and measurement in transmission geometry in the range  $2\theta$  angles  $0^\circ$ – $40^\circ$ ). Powders were prepared as a homogeneous layer less than 0.2 mm thick placed between two thin strips of X-ray amorphous film. The size distribution functions of particles were calculated from SAXS curves in the range of  $2\theta$  angles  $0^\circ$ – $7^\circ$  using the GNOM program;<sup>35</sup> the particles were assumed to be spherical.

The XAFS (EXAFS and XANES) spectra at the  $K$  edge of titanium ( $E_0 \sim 4966 \text{ eV}$ ) were measured in a transmission geometry using two ionization chambers positioned before and after the sample. To optimize the efficiency of performance of the chambers, they were filled with mixtures of nitrogen and argon to absorb 20% of the incident beam in the first chamber and 80% in the second one. To improve the statistical signal-to-noise ratio in the measured spectra, six independent scans were obtained and averaged for each sample. The total acquisition time was 25–30 min per scan. In addition to samples of nanocrystalline titanium dioxide, the reference spectra of anatase and rutile were measured under the same conditions.

IR spectra were recorded with an Infracum FT-02 spectrometer ( $4000$ – $400 \text{ cm}^{-1}$ ) in nujol. Raman spectra were analyzed on an RFS 100/S FT Raman spectrometer (Bruker) using a 1060-nm Nd laser (the power density on the sample surface did not exceed  $50 \text{ W/cm}^2$ ) with a spectral resolution  $2 \text{ cm}^{-1}$ .

Differential scanning calorimetry (DSC) was performed with the use of a DSC204F1 Phoenix (NETZSCH-Geratebau GmbH) instrument with the scanning rate of  $10^\circ\text{C}$  per minute in the Ar atmosphere; accuracy  $\pm 0.1^\circ\text{C}$ .

The microstructure of powdered nanoparticles was studied using a 7500F high-resolution scanning electron microscope. Images were obtained in the low-energy secondary electron mode, because this mode provided the highest resolution (at the 20 and 2 keV energy of the primary beam, the resolution was 1.0 and 1.5 nm, respectively). To exclude the charging effects, a platinum film was deposited on the particle surface by magnetron sputtering (the electrical current was  $30 \mu\text{A}$ , the sputtering time was 20 s, the target to sample distance was 40 cm, and the pressure was 5 Pa). Under these conditions, a platinum film of 5–10 nm thickness was obtained. To exclude artifacts inherited from the deposition of a platinum layer on the particle surface, we performed preliminary experiments on the deposition of platinum onto silicon single crystals under the same conditions. The platinum particle size on single-crystal faces obtained under the specified sputtering conditions was 4–5 nm. We also used GENTLE BEAM mode, intended to ensure high resolution at a low accelerating voltage.

Local measurements of the elemental composition were carried out by EDX spectroscopy using an INCA Penta FETx 3 energy-dispersive X-ray microanalysis system (OXFORD, UK)

coupled with a scanning electron microscope. The calibration (6 iterations) was performed with 2 bands of the  $\text{CoK}$  radiation using cobalt metal as a reference. The quantitative analysis was carried out using the INCA Penta FET program. The standard deviation was  $\pm 0.5\%$ .

UV-vis diffuse reflectance spectra were recorded with a THERMO SPECTRONIC  $\sim$  VISION32 spectrometer in the 350–849 nm range with a 0.49 nm step with the use of thin films (1.0–1.2 mm) of freshly prepared sample.

X-ray photoelectron spectra were obtained with a PHOIBOS 150 MCD spectrometer, monochromatic  $\text{MgK}\alpha$  radiation ( $h\nu = 1253.6 \text{ eV}$ ). The powder was put onto the In surface. The pressure in the sample chamber did not exceed  $3 \cdot 10^{-9}$  Torr, the power of the source was 225 W. X-ray source was placed at  $45^\circ$  with respect to the sample surface. The spectra were recorded with constant transmission energy (30 eV, step 1 eV for a survey spectrum and 10 eV, step 0.1 eV for peaks), 10 atomic layers depth,  $1 \text{ cm}^2$  surface area. The C1s peak (284.8 eV) was used for calibration.

The sorption capacity of the samples with respect to nitrogen at  $-196^\circ \text{C}$  was measured by the static volumetric method (ASAP 2020, Micromeritics); the measurement results were presented in the form of sorption (adsorption and desorption) isotherms. The specific surface of the samples was determined by the Brunauer–Emmett–Teller (BET) method and the comparative method (CM) from the adsorption branch of the isotherm in the ranges of equilibrium relative nitrogen pressures: 0.05–0.35 and 0.4–0.8, respectively. The standard isotherm was obtained for nonporous standard sample ASKh-1-4 (BET specific surface  $4.18 \text{ m}^2 \text{ g}^{-1}$ ), GSO (State Standard Sample) 9735-2010 (set of standard samples of nanostructured aluminum oxide ASKh-1). The average size ( $N_{CM}$ , nm) for spherical particles was calculated with the equation  $N_{CM} = 6 \cdot 10^3 / \rho S_{CM}$ ,<sup>36</sup> where  $\rho = 3.91 \text{ g/m}^3$  is the X-ray density of anatase.<sup>37</sup> The volumes of nanopores ( $V_{np}$ ) and ultranapores ( $V_{unp}$ ) (in this study, nanopores were considered to be pores less than 300 nm in diameter, while the term “ultranapore” was used for pores less than 2 nm in diameter, filled according to the bulk mechanism in the range of low nitrogen pressures) were calculated from the earlier reported equations.<sup>38,39</sup>

### Methyl orange (MO) decolouration

A powdered sample (the weight content was 0.4 g/L) was added to an aqueous solution of the dye (the initial concentration was 0.05 mmol/L); pH  $\sim$  5 for samples 1–9 and 11, pH  $<$  3 for sample 10. The resulting suspension (the volume was 50 mL) was irradiated under visible light (halogen lamp, wavelength range  $>$  450 nm, power of the radiation source 250 W) in an open vessel (the irradiated surface area was  $0.07 \text{ m}^2$ ) with continuous stirring using a magnetic stirrer. The changes in the MO concentration during the reaction ( $c/c_0$ ) were monitored at  $\lambda = 455$ – $470$  and  $500$ – $515 \text{ nm}$  for samples 1–9, 11 and 10, respectively. The model reaction is pseudo-first-order; the rate constant ( $k$ ) is calculated as the slope of the linear semilogarithmic plot of  $c/c_0$  vs the irradiation time  $\tau$ ; in all

cases, the validity of the linear approximation of the kinetic curves characterized by the  $R$  factor was not lower than 0.95; the error of the determination of the reaction rate constant 10%.

## Results and discussion

### Composition, morphology and structure of $\text{H}_2\text{O}_2$ -modified $\text{TiO}_2$

The traditional technique of sensitizing titania is its cold impregnation with various dyes. Sample **1** was prepared similarly by treatment of pre-synthesized and dried anatase with  $\text{H}_2\text{O}_2$ . More effective method is based on introduction of a sensitizer into the reaction mixture while synthesizing titania, e.g. by hydrolysis of titanyl sulfate.<sup>28</sup> Samples **2** and **3** were prepared by prolonged hydrolysis of  $\text{TiOSO}_4 \cdot 2\text{H}_2\text{O}$  followed by treatment with  $\text{H}_2\text{O}_2$ ; NaOH was additionally introduced into the reaction mixture when synthesizing sample **3**.

X-ray powder diffraction patterns of samples **1–3** are presented in Fig. 1. They contain sets of reflections typical for anatase ( $d \sim 3.5 \text{ \AA}$ ,  $\sim 2.38 \text{ \AA}$ ,  $\sim 1.9 \text{ \AA}$ ,  $\sim 1.7 \text{ \AA}$ ,  $\sim 1.5 \text{ \AA}$  and  $\sim 1.35 \text{ \AA}$ ) with the space group  $I4_1/amd$  (JCPDS no. 89-4921). Additional reflections ( $d \sim 5.8 \text{ \AA}$ ,  $\sim 3.1 \text{ \AA}$ ,  $\sim 2.0 \text{ \AA}$ ,  $\sim 1.6 \text{ \AA}$ ) at the pattern of sample **3** indicate the presence of small quantity of  $\beta\text{-TiO}_2$  (JCPDS № 46-1238). Therefore, introduction of NaOH into the reaction mixture seems to stimulate formation of  $\beta\text{-TiO}_2$ .

Cold impregnation of anatase with the  $\text{H}_2\text{O}_2$  solution (sample **1**) results in appearance of  $\text{TiO}_{2-x}(\text{OH})_{2x}\text{yH}_2\text{O}$ , the average size of crystallites remaining  $60 \text{ \AA}$ . Introduction of  $\text{H}_2\text{O}_2$  during synthesis decreases sizes of crystallites down to  $50 \text{ \AA}$  and  $55 \text{ \AA}$  for samples **2** and **3**, respectively. Formation of anatase seems to be preceded by generation of the “ $\eta\text{-TiO}_2$ ” phase; this phase can be isolated if  $\text{TiOSO}_4$  hydrolysis is stopped before transition of “ $\eta\text{-TiO}_2$ ” to anatase.<sup>40–43</sup> Samples **4–7** containing “ $\eta\text{-TiO}_2$ ” were prepared by short-time hydrolysis of titanyl sulfate. Hydrogen peroxide was added along with a coagulant. Samples **4** and **5** were prepared from  $\text{TiOSO}_4 \cdot 2\text{H}_2\text{O}$ ; sample **5** was additionally treated with NaOH.

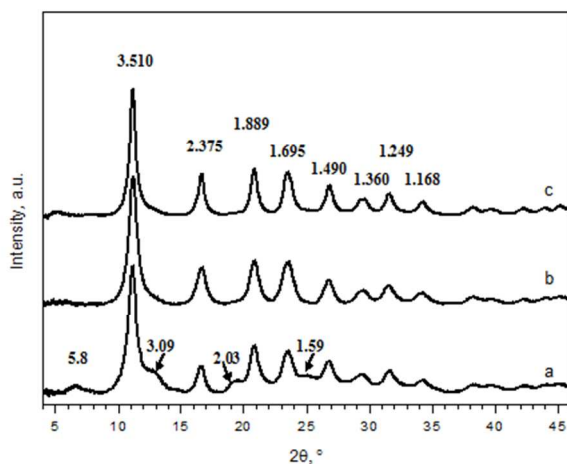


Fig. 1 XRD patterns for samples **3** (a), **2** (b), **1** (c) (synchrotron radiation,  $\lambda = 0.68886 \text{ \AA}$ ). Interplanar distances ( $\text{\AA}$ ) are shown at the peaks.

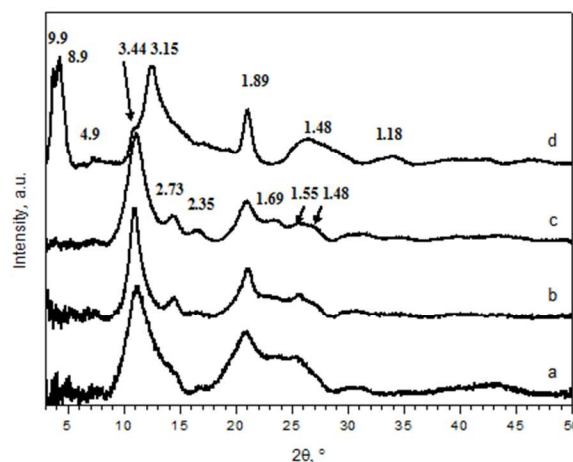


Fig. 2 XRD patterns for samples **7** (a), **4** (b), **6** (c), **5** (d) (synchrotron radiation,  $\lambda = 0.68886 \text{ \AA}$ ). Interplanar distances ( $\text{\AA}$ ) are shown at the peaks.

Samples **6** and **7** were prepared from  $\text{TiOSO}_4 \cdot x\text{H}_2\text{SO}_4 \cdot y\text{H}_2\text{O}$ ; synthesis of sample **7** differs by addition of EDTA.

X-ray powder diffraction patterns of “ $\eta\text{-TiO}_2$ ”-containing samples **4–7** are presented in Fig. 2. The  $\eta\text{-TiO}_2$  phase is characterized by a set of specific reflections ( $d \sim 18 \text{ \AA}$ ,  $2.7 \text{ \AA}$  and  $1.55 \text{ \AA}$ ).<sup>44</sup> The structure of  $\eta\text{-TiO}_2$  is quasi-layered,<sup>40,41</sup> this permits existence of water molecules in the interlayer space; their removal from the crystal structure onto the surface decreases interplanar distances from  $d \sim 21 \text{ \AA}$ <sup>10</sup> to  $\sim 17 \text{ \AA}$ ,<sup>45</sup> along with the corresponding unit cell parameter  $c$ . The other peaks ( $d \sim 3.5 \text{ \AA}$ ,  $\sim 1.9 \text{ \AA}$ ,  $\sim 1.7 \text{ \AA}$ ,  $\sim 1.5 \text{ \AA}$  and  $\sim 1.35 \text{ \AA}$ ) are the same as for anatase. Small number of diffused peaks does not allow solving the “ $\eta\text{-TiO}_2$ ” structure. However, it can be described as a superstructure for anatase,<sup>40,41</sup>  $a \sim b \sim a_0$ ,  $c \sim 2c_0$  ( $a_0$  and  $c_0$  are the unit cell parameters of anatase).

In the patterns of samples **4** and **7**, the specific reflection of anatase ( $d \sim 2.35 \text{ \AA}$ )<sup>10</sup> is absent. Therefore, the samples contain only  $\eta$ -phase; this phase is more ordered in sample **4**, since one of the specific peaks ( $d \sim 2.7 \text{ \AA}$ ) is more pronounced (see Fig. 2). The X-ray diffraction pattern of sample **5** contains, along with reflections of  $\eta\text{-TiO}_2$ , strong reflections of hydrous titania,  $\text{TiO}_{2-x}(\text{OH})_{2x}\text{yH}_2\text{O}$ ,  $y \sim 1$  ( $d \sim 9.9 \text{ \AA}$ )<sup>10</sup> and  $\text{Ti}_4\text{O}_7(\text{OH})_2\text{H}_2\text{O}$  ( $d \sim 8.9 \text{ \AA}$ ,  $4.9 \text{ \AA}$  and  $3.15 \text{ \AA}$ ; JCPDS № 38-0699). Sample **6** contains both  $\eta\text{-TiO}_2$  and anatase, the presence of the latter is supported by the characteristic reflection ( $d \sim 2.35 \text{ \AA}$ ).<sup>10</sup> Phases containing cesium or potassium are absent; they remain in aqueous solutions.

The content of the amorphous component increases in the row: sample **4** < sample **6** < sample **7** < sample **5**. Average sizes of titania crystallites decrease in the same row. This is evidenced by the width of one of specific peaks ( $d \sim 3.5 \text{ \AA}$ ) and shift of the reflections towards larger angles.

The XANES spectra and Fourier transforms of EXAFS for samples **4**, **7** and anatase (Figs. 3 and 4) demonstrate systematic differences in local structure and electronic state of  $\text{Ti}^{4+}$  ions (splitting in the ligand field) in  $\eta\text{-TiO}_2$  and anatase. In particular, comparison of the Fourier transforms of EXAFS shows greater scattering of the Ti–O distances in the first

coordination sphere for  $\eta$ -TiO<sub>2</sub> as compared to anatase. Appearance of additional resonances in the pre-edge region of the XANES spectra (Fig. 3) indicates occurring of the pentacoordinated TiO<sub>5</sub> polyhedra. According to the EXAFS/XANES data, titanium atom in the sample 5 has low-symmetrical environment differing from octahedral.

Therefore, treatment of the product with NaOH (compare samples 4 and 5) effects compositions of the samples and sizes of crystallites. Introduction of EDTA inhibits formation of anatase. Freshly prepared samples 1–7 are yellowish orange due to formation of peroxy complexes on the surface of titania nanoparticles. Samples 1–6 decolorize on storage, indicating decomposition of surface titanium(IV) peroxocomplexes. Sample 7 retains its color on storage; this can be explained by formation of stable peroxyacetic groups.

These results show that any treatment of the already formed titania particles, both anatase and  $\eta$ -TiO<sub>2</sub>, with H<sub>2</sub>O<sub>2</sub> produce surface peroxocomplexes, which gradually destroys on storage. To introduce peroxy groups into the body of titania nanoparticles we pre-treated the initial reagent (titanyl sulfate) with H<sub>2</sub>O<sub>2</sub> and then hydrolyzed the peroxy-containing precursor. Samples 8–11 were prepared by mixing of the H<sub>2</sub>O<sub>2</sub> solution with TiOSO<sub>4</sub>·2H<sub>2</sub>O followed by hydrolysis. Samples 8–10 were prepared from pre-cooled reagents; concentration of H<sub>2</sub>O<sub>2</sub> in the reaction mixture was in the 1 : 1.2 : 2 ratio for 8–10, respectively. Sample 11 was prepared by mixing reagents at room temperature.

The X-ray powder diffraction patterns of samples 8–10 are shown in Fig. 5; Fig. 6 demonstrates the pattern of sample 11 and compares the patterns of samples 2 and 9. There are no specific reflections of  $\eta$ -TiO<sub>2</sub> ( $d \sim 2.7$  Å) and reflections of anatase (particularly,  $d = 1.48$  Å and  $1.27$  Å) in the patterns of samples 8–11. The X-ray powder diffraction patterns of samples 8 and 11 contain no reflection of rutile ( $d \sim 2.48$  Å) (JCPDS № 89-8304). Orthorhombic unit-cell values calculated for sample 11 are  $a = 3.880(5)$ ,  $b = 11.64(2)$ ,  $c = 12.64(1)$  Å.

In the patterns of samples 9 and 10, reflections of rutile are found (Figs. 5 and 6). The X-ray diffraction pattern of sample 10 differs from the pattern of sample 9 by the presence of two reflections,  $d = 3.531$  Å (anatase) (JCPDS no. 89-4921) and  $d = 3.276$  Å (rutile) (JCPDS № 89-8304). Diffused reflection ( $d \sim 3.46$  Å) in the pattern of sample 9 can be considered as an average of two reflections,  $d \sim 3.5$  Å (anatase) and  $\sim 3.3$  Å (rutile).

Interplanar distances from low-angle reflections are smaller for samples 8–11 ( $d \sim 12.7$ – $14.3$  Å) than for  $\eta$ -TiO<sub>2</sub>.<sup>10,45</sup>

Sample 9 contains significant content of an amorphous component; the average crystallite size is 35 Å. Most reflections can be seen on the patterns with both  $\lambda$  values for different X-ray diffraction experiments; however, the reflection with  $d > 10$  Å is absent in the synchrotron experiment with  $\lambda = 0.68886$  Å, but presents at the XRD pattern with  $\lambda = 1.54051$  Å. Analysis of the low-angle scattering for sample 9 indicates nano inhomogeneity and polydispersity;<sup>28</sup> weak ordering with the  $\sim 11.7$  Å period is probable (Fig. 7a).

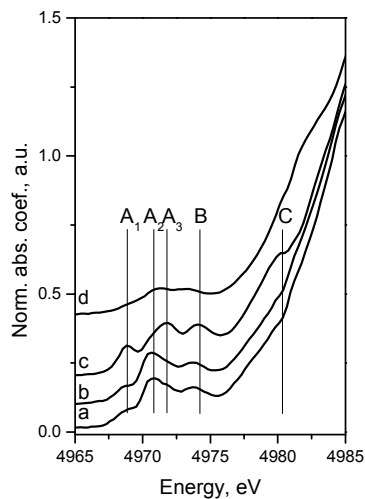
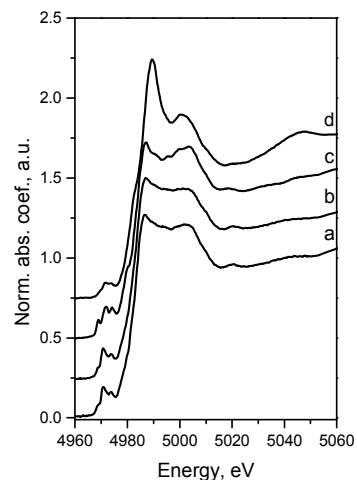


Fig. 3 XANES spectra for samples 4 (a), 7 (b), 2 (anatase) (c) and 9 (d).

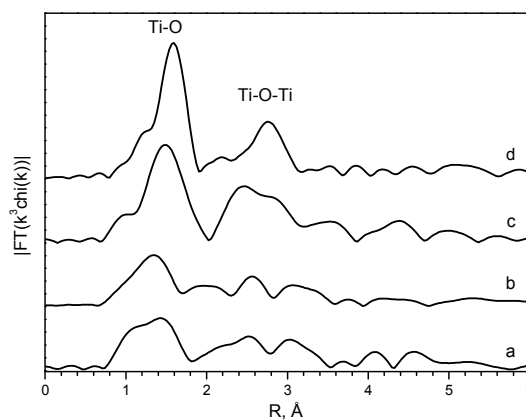


Fig. 4 Fourier transforms of EXAFS for samples 7 (a), 4 (b), 2 (c) and 9 (d).

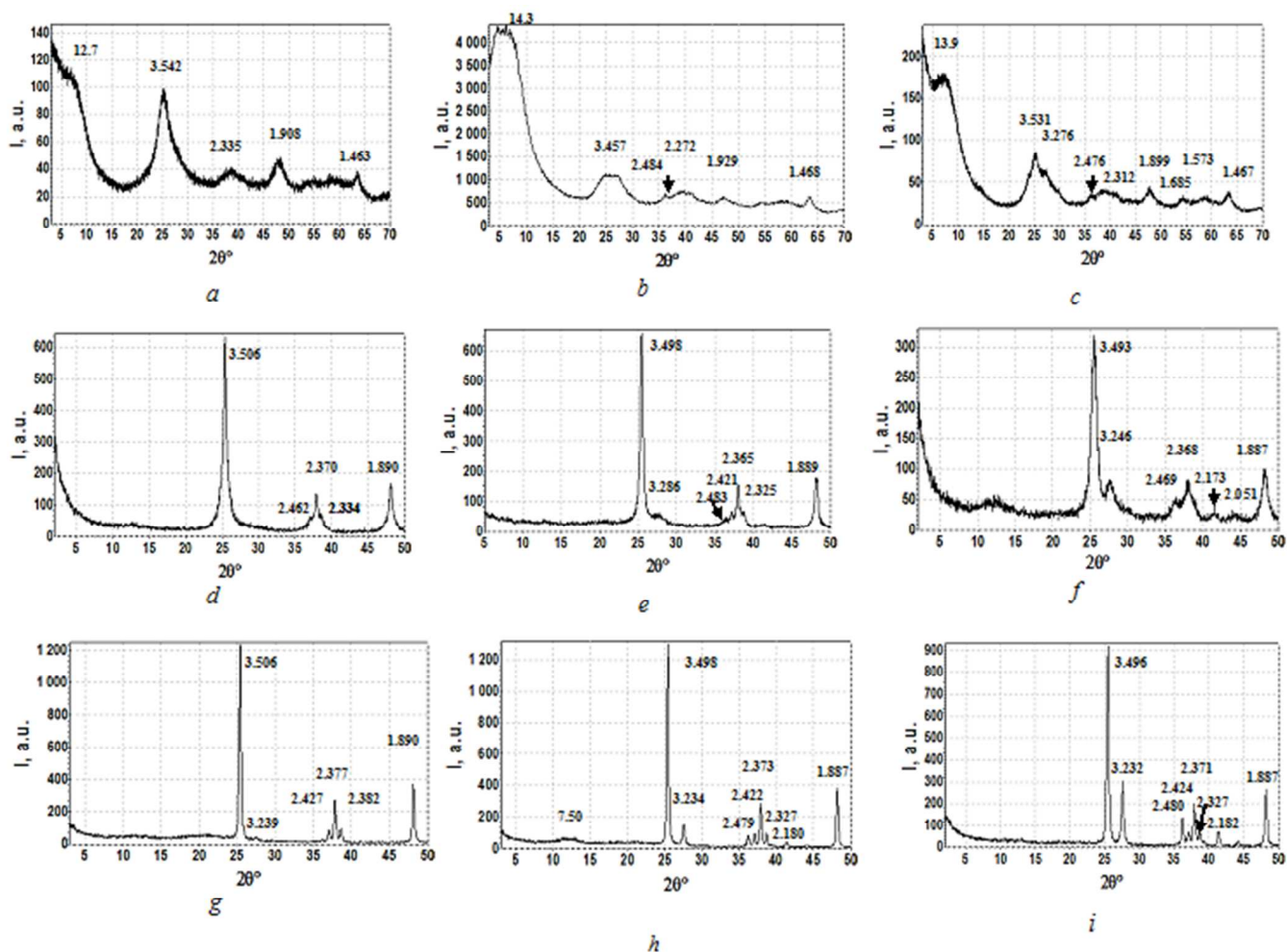


Fig. 5 XRD patterns for samples 8 (a), 9 (b), 10 (c) without annealing; samples 8 (d), 9 (e), 10 (f), annealed at 400°C for 24 h; samples 8 (g), 9 (h), 10 (i), annealed at 800°C for 30 min ( $\lambda = 1.54051 \text{ \AA}$ ). Interplanar distances (Å) are shown at the peaks.

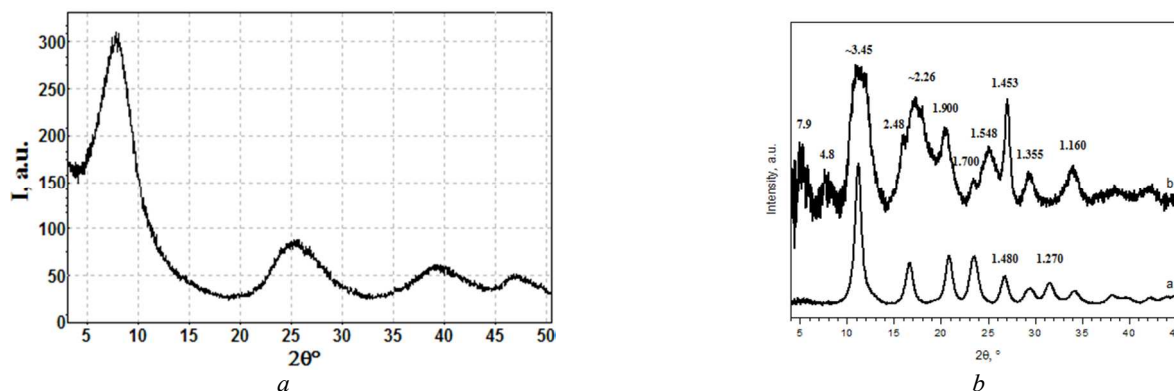


Fig. 6 XRD patterns for a) sample 11 ( $\lambda = 1.54051 \text{ \AA}$ ) and b) samples 2 (1) and 9 (2) (synchrotron radiation,  $\lambda = 0.68886 \text{ \AA}$ ). Interplanar distances (Å) are shown at the peaks.

## ARTICLE

Ratio of nano particles with radii 3.2 and ~1.0 nm is ca. 1 : 4 (Fig. 7b). The EXAFS data show that titanium atom in sample 9 (Fig. 4) has less distorted octahedral surrounding as compared to anatase (sample 2).

The aforementioned results indicate that samples 8–11 contain the phase with the probable unit cell parameters  $a \sim 3.9$ ,  $b \sim 11.6$  Å; variations of the interplanar distance calculated from the low-angle reflections and the corresponding unit cell parameter ( $c \sim 12.6$ – $14.3$  Å) for samples 8–11 can be caused by presence of various quantity of absorbed water molecules in this phase of the  $[\text{TiO}_x(\text{O}_2)_{2-x}(\text{H}_2\text{O})_m]$  composition. This result correlates with the chemical composition of  $[\text{Ti}_2\text{O}_5(\text{OH})_x]^{(x-2)-}$  which was proposed for peroxotitanium acid (and its ions) in aqueous solution and  $\text{TiO}_{1.4}(\text{O}_2)_{0.5}(\text{OH})_{0.2} \cdot 1.34\text{H}_2\text{O}$  for the thin film prepared by its deposition.<sup>46,47</sup>

The DSC curve of sample 11 (Fig. 8) shows an endothermic effect (79.5°C) caused by removal of absorbed water molecules from interlayer space and two exothermic effects (202.3 and 429.2°C) assigned to decomposition of the peroxo phase and formation of anatase, respectively.

The IR spectrum of sample 9 shows weak absorption at 830–890  $\text{cm}^{-1}$  assigned to the stretching vibrations of the O–O bond, which is absent in the spectrum of samples 1 and 2.

Raman spectrum of  $[\text{TiO}_x(\text{O}_2)_{2-x}(\text{H}_2\text{O})_m]$  differs from spectra of anatase and  $\eta$ - $\text{TiO}_2$ . The Raman spectra of anatase samples synthesized by us exhibit bands at about 160 ( $E_g$ ), 520 ( $B_{1g}$ ), and 645 ( $E_g$ )  $\text{cm}^{-1}$ .<sup>40</sup> The Raman spectra of the samples containing  $\eta$ - $\text{TiO}_2$ , along with bands similar to  $E_g$  for anatase (153–168  $\text{cm}^{-1}$ ), exhibit bands at 400–425 and 626–640  $\text{cm}^{-1}$ .<sup>40</sup> These bands are absent in the spectrum of  $[\text{TiO}_x(\text{O}_2)_{2-x}(\text{H}_2\text{O})_m]$ ; its spectrum contains bands at 279, 528 and 914  $\text{cm}^{-1}$ .

Quantitative XPS analysis was performed for sample 8. Typical survey and high-resolution spectra are presented in Fig. 9.

The survey spectrum of the sample 8 particles contains C 1s peak in addition to the Ti 2p and O 1s peaks, confirming the presence of the surface contamination (Fig. 9a).

The Ti 2p<sub>1/2</sub> and Ti 2p<sub>3/2</sub> spin-orbital splitting photoelectrons for sample 8 are located at binding energies of 465.1 and 459.2 eV, respectively (Fig. 9b). The peak separation of 5.9 eV between the Ti 2p<sub>1/2</sub> and Ti 2p<sub>3/2</sub> signals is in excellent agreement with the reported literature values.<sup>48</sup> The FWHM of the Ti 2p<sub>3/2</sub> signal was 1.2 eV for sample 8 (Fig. 9b).

The O 1s signal for sample  $\text{TiO}_2$  particles with peroxo groups is shown in Fig. 9c, indicating a peak at 530.4 eV and a shoulder located toward the side of higher binding energies. The same FWHM and Lorentzian/Gaussian mix values were used in the curve resolution of the individual O 1s peaks in the two spectra. The curve resolved O 1s signal of the sample 8 resulted in a second peak located at a binding energy of 532.4 eV. This secondary peak was assigned to OH<sup>-</sup> and CO<sub>3</sub><sup>2-</sup> species on the surface.

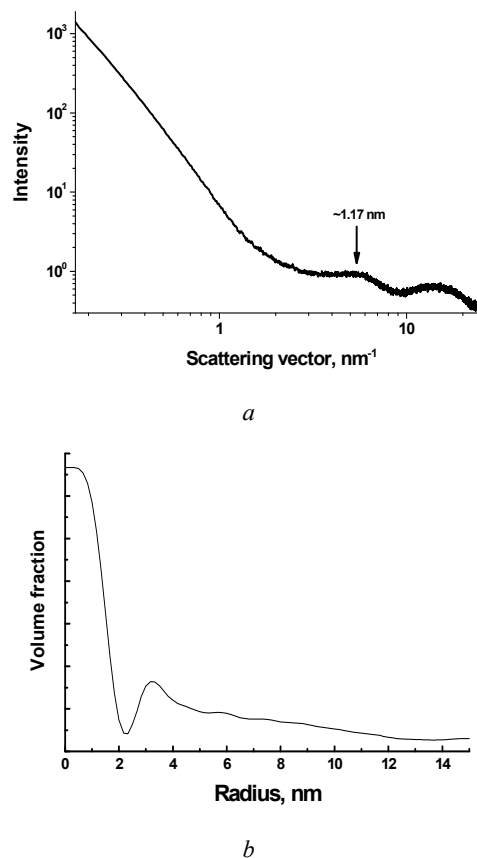


Fig. 7 Curves of the low-angle scattering (a) and distribution of particle sizes in the spherical-shape approximation (b) for sample 9.

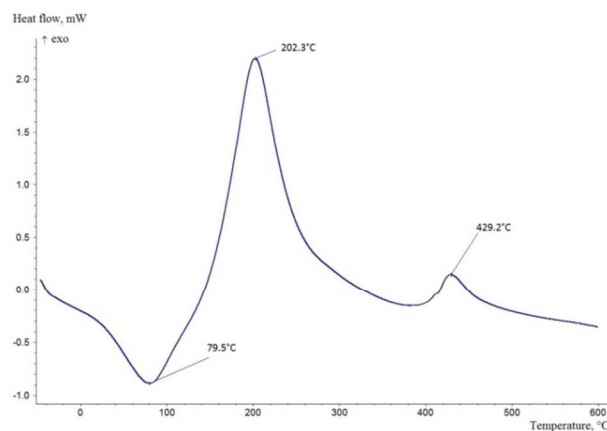
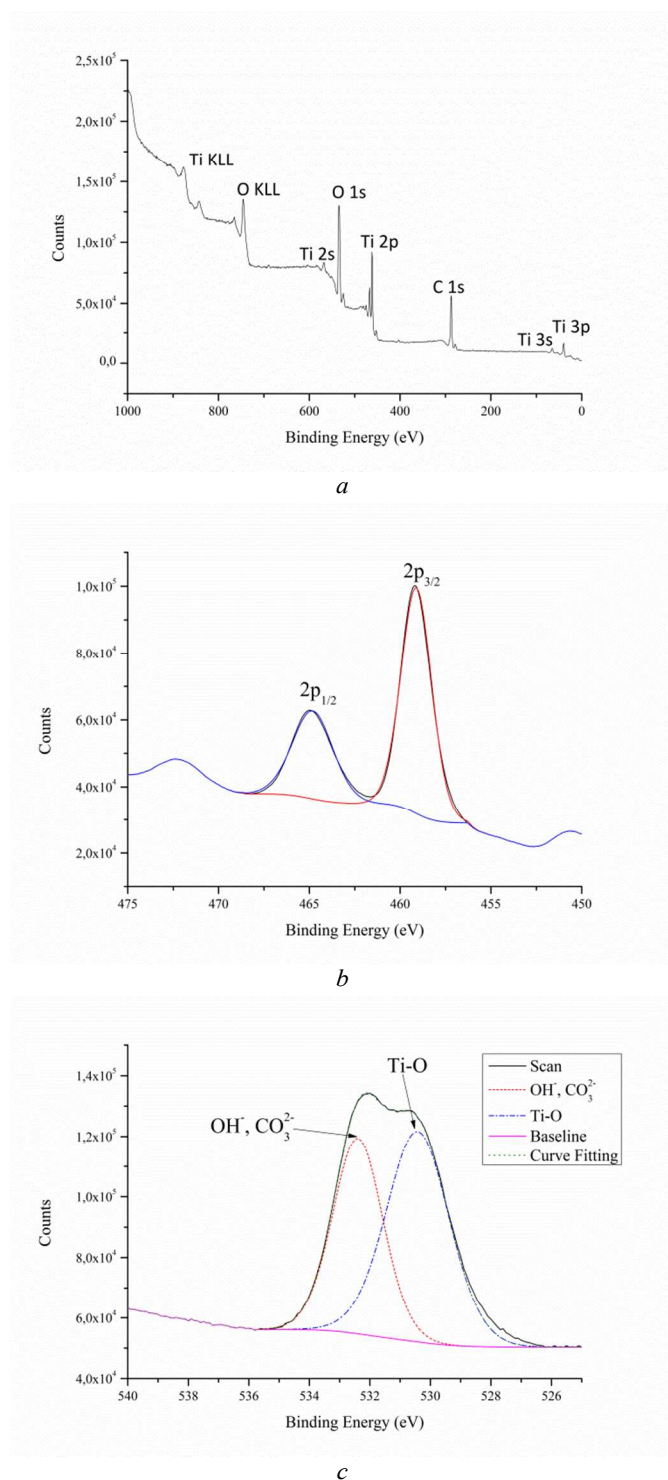


Fig. 8 DSC curve for sample 11.



**Fig. 9** X-ray photoelectron spectra of sample **8**: a) survey Mg K $\alpha$  photoelectron spectra; b) high-resolution XPS spectra of the Ti 2p (no indication for formation of a Ti<sup>3+</sup> sub-oxide can be detected); c) high-resolution XPS spectra of the O 1s peaks.

The values of the FWHM of the lower and higher binding energy peaks were 1.12 and 1.14 eV, respectively. The binding energy difference of 71.2 eV between the observed peak positions of Ti 2p<sub>1/2</sub> and O 1s (oxide) is also in excellent agreement with reported literature values of 72.9–71.2 eV.<sup>49</sup>

X-ray photoelectron spectrum of sample **8** shows that its surface contains Ti (11%, as TiO<sub>2</sub>), O (35%, including 42% as Ti–O and 57% as adsorbed OH<sup>−</sup> and CO<sub>3</sub><sup>2−</sup> ions) and C (54%, including 6% as CO<sub>3</sub><sup>2−</sup> and 93% as C–C) (Fig. 8). We can conclude that there are numerous OH<sup>−</sup>, CO<sub>3</sub><sup>2−</sup> ions and adsorbed water molecules on the surface of nanoparticles.

According to the EDX analysis, the oxygen content decreases in the row sample **10** (O, ~54.8 wt.%; Ti, ~44.3 wt.%; S, ~0.9 wt.%) > sample **9** (O, ~43.5 wt.%; Ti, ~56.2 wt.%; S, ~0.3 wt.%) > sample **2** (O, ~40.1 wt.%; Ti, ~56.4 wt.%; S, ~3.5 wt.%). Extremely high oxygen content in sample **10** can be caused by the presence of large quantity of OH groups on its surface. In contrast to samples **2** and **9**, pH of its water suspension is lower 3.

Nanoparticles in sample **9** and **10** are oval (< 50 nm) and spherical (< 100 nm), respectively (Fig. 10).

Introduction of H<sub>2</sub>O<sub>2</sub> at the first stage of the synthesis results in formation of titanium peroxide; samples **8–11** can be considered as titanium oxide modified with peroxy groups which are included into its crystal structure (and probably present onto its surface). The O<sub>2</sub><sup>2−</sup> groups make titanium coordination octahedron more symmetrical and promote formation of the superstructure based on the anatase structure with the unit cell parameters  $a \sim a_0$ ,  $b \sim 3a_0$  and variable  $c$  depending on water content ( $m$  in [TiO<sub>*x*</sub>(O<sub>2</sub>)<sub>2−*x*</sub>(H<sub>2</sub>O)<sub>*m*</sub>]). The presence of the O<sub>2</sub><sup>2−</sup> groups predictably increases the anatase subunit parameter along the  $y$  axis.

Parameters of samples **8–10** are listed in table 1. For sample **11**, sizes of crystallites are 3.5–5.5 Å; sizes of nanoparticles measured by BET and CM are ~65 and 50 nm, respectively; specific surface determined by BET and CM is 51 and 33 m<sup>2</sup>/g, respectively; specific volumes of ultra- and nanopores are 0.008 and 0.035 cm<sup>3</sup>/g, respectively; band gap 3.07 eV.

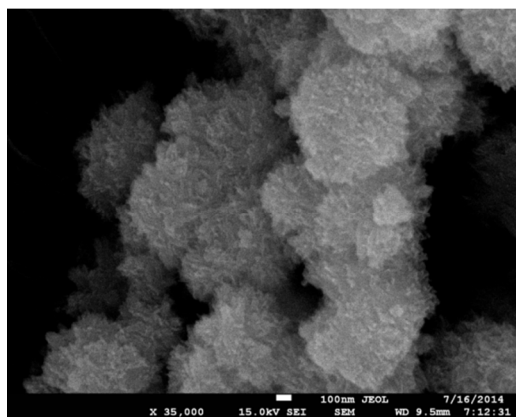
Intensity of the yellow color of samples **8–11** does not reduce on storage for 15 months. They change color on annealing (table 1). The samples decolorize after annealing at 400°C for 24 h or at 800°C for 30 min. The reflection at small angles ( $d \sim 12.7$ – $14.3$  Å) assigned to the [TiO<sub>*x*</sub>(O<sub>2</sub>)<sub>2−*x*</sub>(H<sub>2</sub>O)<sub>*m*</sub>] phase widens and shifts towards larger angles ( $d \sim 10$  Å) on heating to 150°C and disappears on annealing at 400°C indicating decomposition of the phase (Fig. 5).

The samples annealed at 400°C and 800°C contain anatase as a main phase (table 1). X-ray powder diffraction patterns of samples **9** and **10** annealed at 400°C contain reflections (diffuse and sharp, respectively) of the rutile admixture; they become stronger and narrower on annealing at 800°C (Fig. 5). Small quantity of rutile (about 2%) is also found in sample **8** annealed at 800°C.

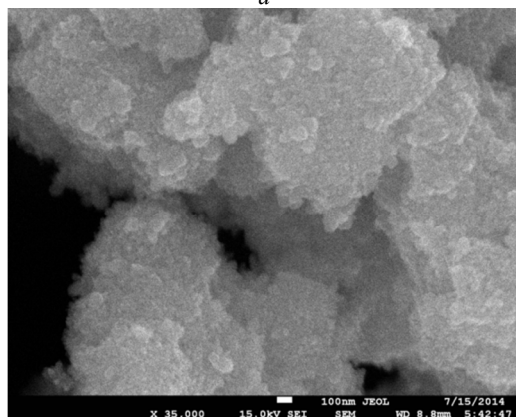
These results agree with the presence of broad exothermic peaks on DSC patterns in the ~200–600°C and ~700–1000°C ranges indicating transitions amorphous hydrous TiO<sub>2</sub> → nano-anatase and nano-anatase → nano-rutile.<sup>50</sup> Increase of the H<sub>2</sub>O<sub>2</sub> concentration favors formation of rutile even at 90–95°C; similar situation was observed earlier.<sup>51</sup>

Table 1. Phase composition, sizes of crystallites ( $D$ ), color and rate constant of MO decolouration under visible light ( $k$ ) for samples 8–10

Parameter	Sample 8	Sample 9	Sample 10
Without annealing			
Phase composition	Peroxo-phase	Peroxo-phase + rutile	Peroxo-phase + rutile
$D$ , Å	38 (20 ~ 25°)	35 (20 ~ 26°)	40 (20 ~ 25°)
Color	Yellow		
$k$ , min <sup>-1</sup>	0.0109	0.0100	0.0037
Annealing at 150°C for 1 h			
Phase composition	Peroxo-phase	Peroxo-phase + rutile	Peroxo-phase + rutile
Color	Pale yellow		
$k$ , min <sup>-1</sup>	0.0014	0.0041	0.00049
Annealing at 400°C for 24 h			
Phase composition	Anatase	Anatase (86%) + rutile (14%)	Anatase (68%) + rutile (32%)
$D$ , Å	145	180 (anatase)	90 (anatase), 60 (rutile)
Color	White		
$k$ , min <sup>-1</sup>	0.00072	0.0014	0.0034
Annealing at 800°C for 0.5 h			
Phase composition	Anatase (98%) + rutile (2%) + amorphous phase	Anatase (83%) + rutile (17%)	Anatase (67%) + rutile (33%)
$D$ , Å	260 (anatase)	275 (anatase), 210 (rutile)	215 (anatase), 205 (rutile)
Color	White		
$k$ , min <sup>-1</sup>	0.00062	0.00066	0.0013



*a*



*b*

Fig. 10 Microphotographs of samples 9 (a) and 10 (b).

### Decolouration of methyl orange

In order to explore the potential application of the H<sub>2</sub>O<sub>2</sub>-modified TiO<sub>2</sub> in the removal of organic contaminants from wastewater, decolouration of MO upon visible light irradiation in the presence of the as-prepared samples was studied. A control experiment was also carried out under identical conditions in the presence of commercial nano-anatase Hombikat UV100 treated with H<sub>2</sub>O<sub>2</sub> in the manner, similar to preparing sample 1.

This model reaction can be used for evaluating activity of various samples, although the lowering of the dye concentration observed in the spectrometer might have been to dye-sensitising effects and/or photocatalysis.

Activity of fresh-prepared samples 1–3 in the reaction of MO decolouration under visible light is higher than of commercial nano-anatase Hombikat UV100 treated with H<sub>2</sub>O<sub>2</sub>; rate constants are 0.0047, 0.0088, 0.0049 and 0.0035 min<sup>-1</sup>, respectively. Maximal activity was found for sample 2. Therefore, treatment of the reaction mixture with H<sub>2</sub>O<sub>2</sub> while preparing anatase from TiOSO<sub>4</sub> (sample 2) is more effective than cold impregnation of anatase, both commercial and self-made. The use of NaOH lowers activity of anatase (sample 3). Samples 1–3 and H<sub>2</sub>O<sub>2</sub>-treated Hombikat UV100 decolorized under storage for 3–4 months at room temperature (due to decomposition of peroxo compounds) and lose their ability to discolor methyl orange under visible light.

Samples 5–7 containing η-TiO<sub>2</sub> also discolor MO; rate constants are 0.017, 0.047 and 0.0049 min<sup>-1</sup>, respectively. Maximal activity was found for freshly-prepared sample 6; treatment with NaOH lowers activity of H<sub>2</sub>O<sub>2</sub>-modified titania. In contrast to samples 4–6 decolorizing under storage for 3–4 months and losing their activity under visible light, color and properties towards MO of sample 7 do not change on storage, but its activity was low initially.

Activity of samples 8, 9 and 11 under visible light is better than of H<sub>2</sub>O<sub>2</sub>-treated commercial Hombikat UV100, activity of sample 10 under visible light being close to activity of the latter; rate constants for samples 8–11 are 0.0100, 0.0109, 0.0037 and 0.0099 min<sup>-1</sup>, respectively (the latter value was obtained with the halogen lamp of lower power, 60 W). Relatively low activity of sample 10 can be caused by large quantity of OH groups on its surface, which are able to interact with anionic SO<sub>3</sub> groups of MO. High activity of samples 8 and 9 does not decrease on storage under light for 15 months. Therefore, these samples are the most promising for MO decolouration under visible light. On annealing, samples 8 and 9 bleach and lower their activity (table 1). Annealing of sample 10 up to 400°C increases its activity; it becomes close to the activity of H<sub>2</sub>O<sub>2</sub>-treated Hombikat UV100. However, further annealing lowers its activity.

As a result, sensitization with H<sub>2</sub>O<sub>2</sub> under various conditions allowed to prepare highly active titania nanoparticles containing anatase, η-TiO<sub>2</sub> and [TiO<sub>x</sub>(O<sub>2</sub>)<sub>2-x</sub>(H<sub>2</sub>O)<sub>m</sub>]. The best activity was found for the freshly-prepared sample 6, containing η-TiO<sub>2</sub>; it is 13-fold higher than for H<sub>2</sub>O<sub>2</sub>-treated

Hombikat UV100 and or exceeds activity of the best earlier reported titania samples with a response to visible light.<sup>27,52-56</sup> Sample 6 is a mixture of amorphous phase, anatase and  $\eta$ -TiO<sub>2</sub>. Higher photocatalytic activity for samples containing three phases of titania (amorphous, anatase, rutile) as compared to mono-phase samples was mentioned earlier.<sup>8</sup> It was explained in terms of increased potential of space charge and the boundary of two phases and localized electronic states of the amorphous phase. Formation of phase junctures between anatase and rutile can increase photocatalytic activity of titania due to a synergic effect, which, however, seems to be absent in Degussa Evonik P25.<sup>57-60</sup> Similar effect can be a reason of high activity of sample 6. Since activity of titania depends on a kind of polymorph, morphology of nanoparticles, bulk and surface composition,<sup>9,55,61,62</sup> varying conditions of synthesis and methods of titania modification allows preparing stable high-vis-active photocatalysts. Samples 8, 9 and 11, containing [TiO<sub>x</sub>(O<sub>2</sub>)<sub>2-x</sub>(H<sub>2</sub>O)<sub>m</sub>], are less active (the rate constant is 3 times larger than for H<sub>2</sub>O<sub>2</sub>-treated Hombikat UV100) as compared to sample 6, but retain their color and activity for a long time.

## Conclusion

With the use of various procedures, we prepared H<sub>2</sub>O<sub>2</sub>-modified titania nanoparticles containing anatase and “ $\eta$ -TiO<sub>2</sub>” (probably, [TiO<sub>2-x</sub>(H<sub>2</sub>O)<sub>m</sub>]) with surface peroxo complexes and [TiO<sub>x</sub>(O<sub>2</sub>)<sub>2-x</sub>(H<sub>2</sub>O)<sub>m</sub>] with peroxo groups in the bulk of crystallites. The [TiO<sub>x</sub>(O<sub>2</sub>)<sub>2-x</sub>(H<sub>2</sub>O)<sub>m</sub>] phase is stable in air for a long time. Its structure seems to be a superstructure to the anatase structure, similar to “ $\eta$ -TiO<sub>2</sub>” [TiO<sub>2-x</sub>(H<sub>2</sub>O)<sub>m</sub>]; it is considered as an ordered substitutional solid solution with replacement of some oxide ions with peroxide ions in “ $\eta$ -TiO<sub>2</sub>” ([TiO<sub>2-x</sub>(H<sub>2</sub>O)<sub>m</sub>]). On annealing, both phases transform to anatase, first nanocrystalline, and then polycrystalline. The both [TiO<sub>x</sub>(O<sub>2</sub>)<sub>2-x</sub>(H<sub>2</sub>O)<sub>m</sub>] and “ $\eta$ -TiO<sub>2</sub>” ([TiO<sub>2-x</sub>(H<sub>2</sub>O)<sub>m</sub>]) phases are prepared only as nano crystals; their crystal structures are stabilized by absorbed water molecules, which affect the unit cell parameter *c*.

Sensitizing titania with hydrogen peroxide by the reported methods results in higher ability to discolor methyl orange under visible light as compared to H<sub>2</sub>O<sub>2</sub>-treated Hombikat UV100. We conclude that high activity of our samples is associated with existence of large amount of titanium peroxo complexes both on the surface and in the bulk of the titania particles along with formation of the mixed-phase samples.

The samples containing peroxo groups in the bulk of the titania nanoparticles show significantly higher stability as compared to the samples containing surface peroxo groups.

## Acknowledgements

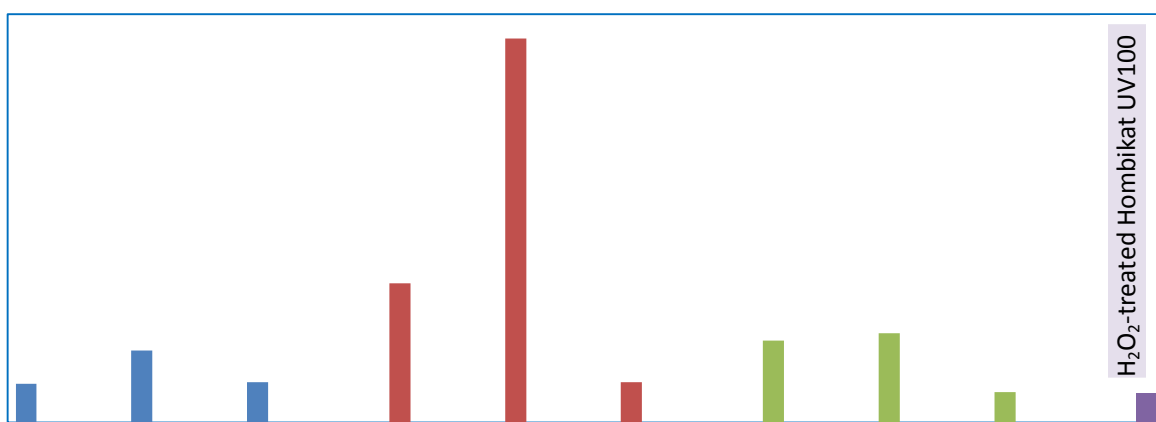
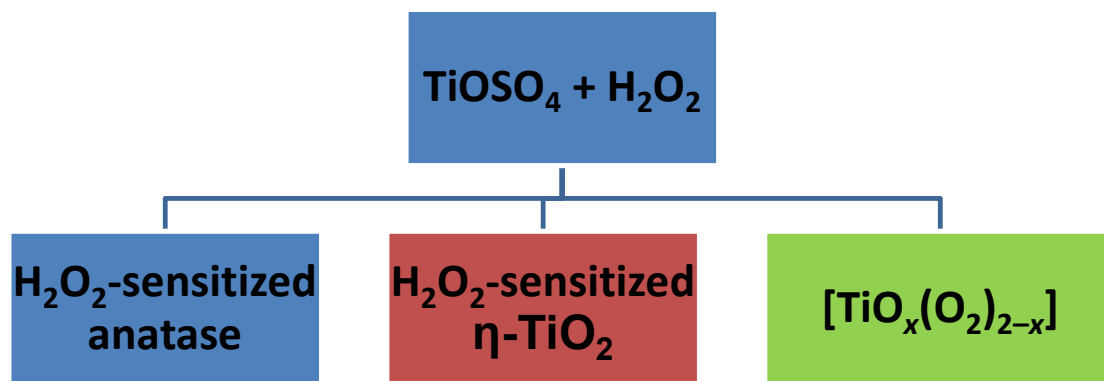
This work was supported by the Russian Foundation for Basic Research (project no. 13-03-00367).

## Notes and references

- <sup>a</sup> Lomonosov Moscow University of Fine Chemical Technology, 86, Vernadskogo pr., 119571 Moscow, Russia.  
<sup>b</sup> Institute of Problems of Chemical Physics of Russian Academy of Science in Chernogolovka, 1, Semenova pr., 142432 Chernogolovka, Moscow region, Russia  
<sup>c</sup> Scientific Center in Chernogolovka of Russian Academy of Science, 9, Lesnaya ul., 142432 Chernogolovka, Moscow region, Russia  
<sup>d</sup> NRC “Kurchatov Institute”, 1, Akademika Kurchatova pl., 123182 Moscow, Russia.  
<sup>e</sup> Karpov Institute of Physical Chemistry, Build. 6, 3–1/12 Obuha per., 105064 Moscow, Russia.

- 1 Y. Lan, Y. Lu and Z. Ren, *Nano Energy*, 2013, **2**, 1031.
- 2 K. Hashimoto, H. Irie and A. Fujishima, *Jpn. J. App. Phys.*, 2005, **44**, 8269.
- 3 I. K. Konstantinou and T. A. Albanis, *Appl. Catalysis B: Environmental*, 2004, **49**, 1.
- 4 B. Zielińska and A. W. Morawski *Appl. Catalysis B: Environmental*, 2005, **55**, 221.
- 5 O. Legrini, E. Oliveros and A. M. Braun, *Chem. Rev.*, 1993, **93**, 671.
- 6 O. Carp, C. L. Huisman and A. Reller, *Progr. Solid State Chem.*, 2004, **32**, 33.
- 7 Y. Matsumoto, U. Unal, N. Tanaka, A. Kudo and H. Kato, *J. Solid State Chem.*, 2004, **177**, 4205.
- 8 Z. R. Ismagilov, L. T. Tsikoza, N. V. Shikina, V. F. Zarytova, V. V. Zinoviev and S. N. Zagrebelnyi, *Russ. Chem. Rev.*, 2009, **78**, 873.
- 9 A. Fujishima, K. Hashimoto and T. Watanabe, *TiO<sub>2</sub> photocatalysis. Fundamentals and applications*, 1st ed., Tokyo: BKC, 1999.
- 10 M. Dadachov, *US Pat.* 0 171 877, 2006.
- 11 A. N. Banerjee, *Nanotechnol. Sci. Appl.*, 2011, **4**, 35.
- 12 D. Pei and J. Luan, *Int. J. Photoenergy*, 2012, **2012**, Article ID 262831, 13 pages.
- 13 X. Zhang, U. Veikko, J. Mao, P. Cai and T. Peng, *Chem. Eur. J.*, 2012, **18**, 12103.
- 14 R. Cai, K. Itoh and C. Sun, *MRS Proceedings*, 2005, **900**, 0900-O13-05, doi:10.1557/PROC-0900-O13-05.
- 15 G. Schwarzenbach, J. Mühlebach and K. Müller, *Inorg. Chem.*, 1970, **9**, 2381.
- 16 F. Wu, X. Li, Z. Wang, L. Wu, H. Guo, X. Xiong, X. Zhang and X. Wang, *Int. J. Miner. Process*, 2011, **98**, 106.
- 17 N. Sasirekha, B. Rajesh and Y. W. Chen, *Thin Solid Films*, 2009, **518**, 43.
- 18 M. V. Shankar, T. Kako, D. F. Wang and J. H. Ye, *J. Colloid Interf. Sci.*, 2009, **331**, 132.
- 19 L. Ge, M. X. Xu, H. B. Fang and M. Sun, *Appl. Surf. Sci.*, 2006, **253**, 720.
- 20 M. Kobayashi, H. Kato and M. Kakihana *Nanomater. Nanotechnol.*, 2013 **3**, Art. 23.
- 21 Y. Gao, H. Luo, S. Mizusugi and M. Nagai, *Cryst. Growth Des.*, 2008, **8**, 1804.
- 22 V. Etacheri, M. K. Seery, S. J. Hinder and S. C. Pillai, *Adv. Funct. Mater.*, 2011, **21**, 3744.
- 23 L. Ge and M. Xu, *J. Sol-Gel Sci. Technol.*, 2007, **43**, 1.
- 24 L. Ge, M. Xu, L. E. Y. Tian and H. Fang, *Key Eng. Mater.*, 2005, **280–283**, 809.

- 25 S. Karuppuchamy and J. M. Jeong, *J. Oleo Sci.*, 2006, **55**, 263.
- 26 R. S. Sonawane, S. G. Hegde and M. K. Dongare, *Mater. Chem. Phys.*, 2003, **77**, 744.
- 27 J. Zou, J. Gao and Y. Wang, *J. Photochem. Photobiol. A: Chemistry*, 2009, **202**, 128.
- 28 E. Savinkina, L. Obolenskaya and G. Kuzmicheva, *Appl. Nanosci.*, 2015, **5**, 125.
- 29 L. N. Obolenskaya, G. M. Kuz'micheva, E. V. Savinkina, N. V. Sadvovskaya, A. V. Zhilkina, N. A. Prokudina and V. V. Chernyshev, *Rus. Chem. Bull.*, 2012, **61**, 2049.
- 30 V. V. Zhurov and S. A. Ivanov, *Crystallogr. Rep.*, 1997, **42**, 202.
- 31 B. E. Warren *X-Ray Diffraction*, New York: Dower Publications, 1990.
- 32 A. A. Chernyshov, A. A. Veligzhanin and Y. V. Zubavichus, *Nucl. Instr. Meth. Phys. Res. A*, 2009, **603**, 95.
- 33 N. N. Trofimova, A. A. Veligzhanin, V. Y. Murzin, A. A. Chernyshov, E. V. Khramov, V. N. Zabluda, I. S. Edelman, Y. L. Slovokhotov and Y. V. Zubavichus, *Rus. Nanotechnology*, 2013, **8**, 108.
- 34 A. P. Hammersley, S. O. Svensson, M. Hanfland, A. N. Fitch and D. Häusermann, *High Press. Res.*, 1996, **14**, 235.
- 35 D. I. Svergun *J. Appl. Crystallogr.*, 1992, **25**, 495.
- 36 V. A. Dzis'ko, A. P. Karnaukhov and D. V. Tarasova, *Physicochemical fundamentals for the synthesis of oxide catalysts*, Nauka, Novosibirsk, 1978.
- 37 P. Villars, *Material Phases Data System (MPDS)*, CH-6354 Vitznau, Switzerland; SpringerMaterials; sd\_1627926 (Springer-Verlag GmbH, Heidelberg), 2014.
- 38 ISO 15901-2:2006 (E). *Pore Size Distribution and Porosity of Solid Materials by Mercury Porosimetry and Gas Adsorption. Part 2: Analysis of Mesopores and Macropores by Gas Adsorption*
- 39 ISO 15901-3:2007. *Pore Size Distribution and Porosity of Solid Materials by Mercury Porosimetry and Gas Adsorption. Part 3: Analysis of Micropores by Gas Adsorption*
- 40 G. M. Kuz'micheva, E. V. Savinkina, L. N. Obolenskaya, L. I. Belogorokhova, B. N. Mavrin, M. G. Chernobrovkin and A. I. Belogorokhov, *Crystallogr. Rep.*, 2010, **55**, 866.
- 41 G. M. Kuz'micheva, E. V. Savinkina, L. I. Belogorokhova, B. N. Mavrin, V. R. Flid, A. G. Yakovenko and A. I. Belogorokhov, *Rus. J. Phys. Chem. A*, 2011, **85**, 1037.
- 42 L. N. Obolenskaya, G. M. Kuz'micheva, E. V. Savinkina, N. A. Prokudina, V. V. Chernyshov and N. V. Sadvovskaya, *Rus. J. Inorg. Chem.*, 2012, **57**, 1177.
- 43 E. V. Savinkina, G. M. Kuz'micheva, L. N. Obolenskaya and E. N. Domoroshchina, *RU Pat. 2 469 954*, 2011.
- 44 G. Kuzmicheva, E. Savinkina, L. Obolenskaya, Y. Zubavichus, V. Murzin and V. Podbelskiy, Proc. of the 8th European Meeting on Solar Chemistry and Photocatalysis: Environmental Applications – SPEA8 (Thessaloniki, Greece) p. 61, 2014.
- 45 G. M. Kuz'micheva, A. A. Gainanova, A. S. Orekhov, V. V. Klechkovskaya, N. V. Sadvovskaya and V. V. Chernyshev, *Cryst. Rep.*, 2014, **59**, 916.
- 46 J. Mühlbach, K. Müller and G. Schwarzenbach, *Inorg. Chem.*, 1970, **9**, 2381.
- 47 Y. Gao, Y. Masuda, Z. Peng, T. Yonezawa and K. Koumoto, *J. Mater. Chem.*, 2003, **13**, 608.
- 48 E. McCafferty and J. P. Wightman, *Surf. Interface Anal.*, 1998, **26**, 549.
- 49 J. Chastian, Ed., *Handbook of X-ray Photoelectron Spectroscopy; Physical Electronics*, MN; Eden Prairie, 1992.
- 50 A. Gainanova, G. Kuz'micheva, E. Kopylova and A. Dorokhov. Proc. of the 14<sup>th</sup> European Conference of Solid State Chemistry (ECSSC14) (Bordeaux, France) p. 127, 2013
- 51 L. N. Obolenskaya, E. N. Domoroshchina, E. V. Savinkina and G. M. Kuzmicheva, *Fund. Res.*, 2013, **1**, 796.
- 52 N. Guiettai and H. A. Amar, *Desalination*, 2005, **185**, 427.
- 53 X.-T. Zhou, H.-B. Ji and X.-J. Huang, *Molecules*, 2012, **17**, 1149.
- 54 F. Chen, W. Zou, W. Qu and J. Zhang, *Catal. Comm.*, 2009, **10**, 1510.
- 55 R. S. Varma, B. Baruwati and J. Virkutyte, *US Pat. 0 266 136*, 2011.
- 56 E. V. Savinkina, L. N. Obolenskaya and G. M. Kuz'micheva. *RU Pat. 2 520 100*, 2014.
- 57 F. Yu, Y. Wang, H. Tang, Y. Zhang, C. Jin, X. Liu, M. Li and J. Wang, *Catal. Comm.*, 2014, **51**, 46.
- 58 J. Zhang, Q. Xu, Z. C. Feng, M. J. Li and C. Li, *Angew. Chem. Int. Ed.*, 2008, **47**, 1766.
- 59 D. O. Scanlon, C. W. Dunnill, J. Buckeridge, S. A. Shevlin, A. J. Logsdail, S. M. Woodley, C. R. A. Catlow, M. J. Powell, R. G. Palgrave, I. P. Parkin, G. W. Watson, T. W. Keal, P. Sherwood, A. Walsh and A. A. Sokol, *Nature Mater.*, 2013, **12**, 798.
- 60 Y. K. Kho, A. Iwase, W. Y. Teoh, L. Madler, A. Kudo and R. Amal, *J. Phys. Chem. C*, 2010, **114**, 2821.
- 61 C. Kormann, D. W. Bahnemann and M. R. Hoffmann, *J. Phys. Chem.*, 1988, **92**, 5196.
- 62 H. Lin, C. P. Huang, W. Li, C. Ni, S. I. Shah and Y.-H. Tseng, *Appl. Catal. B: Environmental*, 2006, **68**, 1.



Photocatalytic activity under visible light